arXiv:2609.13341v1 [q-bio.PE] 11 Sep 2026

GrassTop: Grassmannian k-mer Topology for Viral Classification and Phylogenetic Analysis

Xiang Xiang Wang[1], Guo-Wei Wei[1,2,3*]
[1] Department of Mathematics,
University of Georgia, Athens, GA 30602, USA.
[2] Department of Biochemistry and Molecular Biology,
University of Georgia, Athens, GA 30602, USA.
[3] School of Computing,
University of Georgia, Athens, GA 30602, USA.

Abstract

We introduce GrassTop, a genome representation that integrates Grassmann manifolds and algebraic topology for viral classification and phylogenetic analysis. The framework begins by constructing multiscale topological and spectral descriptors of (k)-mer positional patterns. It then extracts a low-rank subspace that summarizes variation across the filtration and compares genomes using a Grassmannian distance. Although the reported implementation uses the chordal distance, the framework is not restricted to this particular choice. We evaluate GrassTop on four families of viral classification datasets, four phylogenetic clustering datasets, and a sequence perturbation experiment. Under the reported 5-nearest-neighbor protocol, GrassTop achieves higher scores than five published alignment-free reference methods across all reported classification metrics and datasets. Its UPGMA (unweighted pair-group method using arithmetic averages) trees achieve an average label purity of 1.0 on every phylogenetic dataset. The perturbation experiment provides a more nuanced result: the subspace representation differs most clearly from direct comparison of the unprojected feature matrices for SARS-CoV-2, whereas the differences are smaller or non-monotonic for the other datasets. Overall, these results support GrassTop as an effective topological-geometric representation for viral classification and phylogenetic analysis.

Keywords: Grassmannian, k-mer topology, persistent homology, alignment-free genome analysis, phylogenetics.

1 Introduction

Viral classification and phylogenetic analysis are essential for understanding the diversity, evolution, and transmission of viruses. Viral classification provides a systematic framework for organizing viruses based on their genomic, structural, and evolutionary characteristics, enabling the identification of emerging or previously unrecognized viral lineages [17]. Viral phylogenetics reconstructs evolutionary relationships among viral sequences, helping reveal patterns of mutation, recombination, host adaptation, transmission, and geographic spread [5]. Together, they provide a critical foundation for surveillance, outbreak investigation, prediction of viral evolution, vaccine and antiviral development, and assessment of emerging infectious-disease risks.

*Corresponding author: guowei.wei@uga.edu

Due to the extended lengths of genomes, large language models (LLMs) cannot be directly applied. Effective alignment free methods are commonly used in the field, including Nature Vector Method (NVM) [25], Feature Frequency Profile with Jensen-Shannon (FFP-JS) divergence [10,23] and with Kullback-Leibler (FFP-KL) [27], Markov k-string model (MKS) [20], and Fourier Power Spectrum (FPS) [7]. CAFE is a model-based alignment-free approach that further derives explicit evolutionary distances from k-mer frequency statistics under substitution assumptions [14]. Although efficient, many existing methods do not adequately capture positional and structural information, which limits their performance in the analysis of genetic variants [32].

This work introduces GrassTop as a new geometry and topology-based approach for viral classification and phylogenetic analysis. GrassTop is a genome representation in which each sequence is mapped to a low-rank subspace on a Grassmannian. The representation is constructed from multiscale algebraic topology and topological spectral theory of k-mer positions along the sequence. It is therefore intended to retain the organization of the descriptor collection across a filtration while replacing alignment comparison by subspace analysis. Once represented, two genomes can be compared with a distance defined on the Grassmannian.

The construction connects two existing ideas. The first is k-mer topology, which uses persistent homology [33] and persistent Laplacian [13, 28] to describe the positional relationship associated genetic sequences [8]. This topological sequence analysis (TSA) of biological sequences [12] is a generalization of the earlier topological data analysis (TDA) of biomolecular structures [18, 19, 30]. The k-mer topology provides multiple curves over a common filtration and across a selected set of k-mer orders, and this construction belongs to a broader line of work applying algebraic topology, topological spectral theory, and commutative algebra to interpretable analysis of real-world data [21, 24, 26, 29]. Compared with frequency-based k-mer methods, k-mer topology incorporates crucial positional information. The second is subspace-based genome representation via Grassmannians [9]. Li et al. mapped frequency chaos-game representations to Grassmannians and compared their column spaces geometrically [11], part of a broader trend toward differential-geometry-based representation learning for biological network and single-cell data [4], as well as geometric and geometric-deep-learning models of molecular structure [16, 22]. GrassTop differs in the information supplied to the subspace construction: it uses topological and spectral summaries of k-mer positional patterns rather than frequency chaos-game representations. Accordingly, the contribution of this paper is not the first use of a Grassmannian for genomes, but a Grassmannian formulation of multiscale k-mer topology descriptors that draws on both of these methodological threads.

GrassTop normalizes and assembles k-mer topology descriptor blocks, extracts a rank-r subspace, and represents the genome by that subspace. The experiments instantiate this general construction with the configuration described in Section 4.1. We study three questions: whether the representation supports viral-family classification, whether its distances recover labelled groups in phylogenetic clustering, and how its response to sequence perturbations differs from direct comparison of the corresponding descriptors.

The evaluation uses four benchmark NCBI viral-family datasets, four phylogenetic datasets, and sequence perturbation rates from 10^{-4} to 0.4 [8]. Classification is assessed with a repeated 5-nearest-neighbor protocol and six metrics; clustering is assessed with UPGMA tree purity [26]; and the response to perturbation is assessed by label preservation, self preservation, and the normalized distance to the original sequence. These experiments evaluate the complete representation on the stated tasks. They do not by themselves establish that a Grassmannian representation is preferable for every genome dataset or every choice of input representation.

The remainder of this paper is organized as follows. Section 2 reviews the necessary background on k-mer topology features and Grassmannians. Section 3 introduces the GrassTop framework that maps a sequence's stacked topological feature blocks onto a Grassmannian point and presents the chordal distance used in the reported experiments. Section 4 describes the experimental setup and reports classification, phylogenetic-clustering, and perturbation results. Section 5 discusses the findings, and Section 6 concludes

the paper.

2 Mathematical Foundations

This section introduces the mathematical objects used throughout the paper: the k-mer topology feature blocks of Hozumi & Wei [8], and the Grassmannian on which the GrassTop representation of Section 3 is built.

2.1 k-mer topology features

The input features of GrassTop are derived from the k-mer topology construction of Hozumi and Wei [8]. The following formulation summarizes the components of that construction required for the Grassmannian representation.

Let $S = s_1 s_2 \cdots s_N$, with $s_i \in \{A, C, G, T\}$, and let ℓ be one of the 4^k possible k-mer types. If ℓ occurs n_ℓ times, Hozumi and Wei define the k-mer-specific position function [8, Definition 4.2]

$$S^\ell : [n_\ell] \longrightarrow \mathbb{N}, \qquad i \longmapsto S^\ell(i),$$

where $S^\ell(i)$ is the starting position of the ith occurrence of ℓ and $[n_\ell] = \{1, \ldots, n_\ell\}$. The associated k-mer-specific position-distance matrix is

$$D^\ell = \{d^\ell_{ij}\}, \qquad d^\ell_{ij} = \left|S^\ell(i) - S^\ell(j)\right|, \quad 1 \le i, j \le n_\ell, \tag{1}$$

as in [8, Section 4.1.1]. Thus, the input records pairwise separations between occurrences of the same k-mer rather than only its total count.

2.1.1 Persistent Laplacian features

The filtration radius is denoted by ρ rather than by r, as in [8], because r denotes the retained Grassmannian rank below. For $\rho \ge 0$, Hozumi and Wei construct the ℓ-specific degree-zero graph Laplacian [8, Section 4.1.2]

$$(L^\ell_\rho)_{ij} = \begin{cases} -1, & i \ne j \text{ and } d^\ell_{ij} \le \rho, \\ \#\{j \ne i : d^\ell_{ij} \le \rho\}, & i = j, \\ 0, & \text{otherwise.} \end{cases} \tag{2}$$

Equivalently, $L^\ell_\rho = \mathsf{D}^\ell_\rho - A^\ell_\rho$, the standard combinatorial Laplacian of the threshold graph at radius ρ [1]. These graphs are nested as ρ increases, giving the filtration used for degree-zero persistent homology [3, 33]. The eigenvalues are ordered as

$$0 = \lambda^\ell_1(\rho) \le \cdots \le \lambda^\ell_{n_\ell}(\rho).$$

The multiplicity of zero, rather than the number of nonzero eigenvalues, is the Betti-0 number:

$$\beta^\ell_0(\rho) = \dim \ker L^\ell_\rho. \tag{3}$$

This equality follows from the standard graph-Laplacian kernel theorem [1, 28]. Let $m_\ell(\rho) = n_\ell - \beta^\ell_0(\rho)$ and write the positive eigenvalues as $0 < \lambda^{\ell,+}_1(\rho) \le \cdots \le \lambda^{\ell,+}_{m_\ell(\rho)}(\rho)$. Two descriptors considered by Hozumi and Wei are

$$B^\ell(\rho) = \beta^\ell_0(\rho), \qquad E^\ell(\rho) = \lambda^{\ell,+}_1(\rho),$$

collected over increasing radii to form k-mer-specific curves [8, Section 4.1.2].

The present study additionally considers the mean and standard deviation of the positive spectrum. These quantities are not definitions introduced by Hozumi and Wei; they are persistent spectral summary statistics of the type described by Meng and Xia [15]:

$$\mathrm{MEANP}^{\ell}(\rho) = \frac{1}{m_\ell(\rho)} \sum_{j=1}^{m_\ell(\rho)} \lambda_j^{\ell,+}(\rho), \tag{4}$$

$$\mathrm{STDP}^{\ell}(\rho) = \left[\frac{1}{m_\ell(\rho)} \sum_{j=1}^{m_\ell(\rho)} \left(\lambda_j^{\ell,+}(\rho) - \mathrm{MEANP}^{\ell}(\rho)\right)^2 \right]^{1/2}. \tag{5}$$

The three positive-spectrum descriptors are set to zero when no positive eigenvalue exists; all four descriptors are set to zero when ℓ is absent.

Definition 2.1 (k-mer topology feature block)**.** For each descriptor g selected for analysis and sampled at T increasing radii $\rho_1^{(k)}, \ldots, \rho_T^{(k)}$, the 4^k k-mer-specific curves are arranged into

$$G_{S,g}^{(k)} \in \mathbb{R}^{4^k \times T}, \qquad \left[G_{S,g}^{(k)}\right]_{\ell,t} = g^{\ell}\left(\rho_t^{(k)}\right),$$

whose rows follow the lexicographic order of the k-mer types and whose columns follow the filtration order.

Definition 2.1 introduces only the matrix arrangement used by GrassTop; the position distances, Laplacians, and source curves are those defined above. The construction is not restricted to a prescribed set of spectral descriptors. In the experiments reported here, the selected descriptors are $g \in \{B, E, \mathrm{MEANP}, \mathrm{STDP}\}$.

2.2 Grassmannians and subspace distances

For integers $1 \le r < n$, the collection of r-dimensional linear subspaces of $\mathbb{R}^n$ forms a Grassmannian. Its representation by orthonormal frames, the identification of subspaces through the singular value decomposition, and the comparison of subspaces through principal angles are summarized below [2, 31].

Definition 2.2 (Grassmannian [2, 31])**.** The Grassmannian $\mathrm{Gr}(r, n)$ is the set of all r-dimensional linear subspaces of $\mathbb{R}^n$. If

$$\mathrm{St}(r, n) = \{U \in \mathbb{R}^{n \times r} : U^\top U = I_r\}$$

is the Stiefel manifold of orthonormal r-frames, then

$$\mathrm{Gr}(r, n) \cong \mathrm{St}(r, n)/\mathrm{O}(r).$$

Consequently, $U, U' \in \mathrm{St}(r, n)$ represent the same Grassmannian point if and only if $U' = UO$ for some $O \in \mathrm{O}(r)$.

2.2.1 Singular value decomposition

Let $Z \in \mathbb{R}^{n \times T}$ and $1 \le r < \min(n, T)$. A singular value decomposition of Z is [6]

$$Z = U \Sigma V^\top, \qquad \sigma_1(Z) \ge \cdots \ge \sigma_{\min(n,T)}(Z) \ge 0,$$

where U and V are orthogonal matrices and the singular values are ordered nonincreasingly. The first r left singular vectors form $U_r \in \mathrm{St}(r, n)$, and their span defines the left singular subspace associated with the r largest singular values:

$$\mathcal{U}_r(Z) = \mathrm{span}(U_r) \in \mathrm{Gr}(r, n). \tag{6}$$

The truncated factorization $U_r \Sigma_r V_r^\top$ is a best rank-r approximation of Z in the Frobenius norm by the Eckart–Young theorem [**?**, 6]. The subspace $\mathcal{U}_r(Z)$ is uniquely determined when $\sigma_r(Z) > \sigma_{r+1}(Z)$; if the two singular values are equal, the choice of an r-dimensional subspace within the corresponding singular subspace need not be unique [6].

2.2.2 Principal angles and chordal distance

Distances between Grassmannian points can be expressed through principal angles. For $\mathcal{U} = \mathrm{span}(U)$ and $\mathcal{V} = \mathrm{span}(V)$ in $\mathrm{Gr}(r, n)$, their principal angles $0 \le \theta_1 \le \cdots \le \theta_r \le \pi/2$ satisfy

$$\cos\theta_i = \sigma_i(U^\top V), \qquad i = 1, \ldots, r, \tag{7}$$

where the singular values are ordered nonincreasingly [?, 31]. Principal angles depend only on the two subspaces, not on the particular orthonormal bases used to represent them.

The chordal distance between two points $\mathcal{U}, \mathcal{V} \in \mathrm{Gr}(r, n)$ is defined in terms of their principal angles [31, Table 2]. For orthonormal basis matrices U and V, its equivalent principal-angle and projection-matrix forms are

$$d_{\mathrm{chord}}(\mathcal{U}, \mathcal{V}) = \left(\sum_{i=1}^{r} \sin^2\theta_i\right)^{1/2} = \frac{1}{\sqrt{2}} \left\| UU^\top - VV^\top \right\|_F, \tag{8}$$

where $\|A\|_F = (\mathrm{tr}(A^\top A))^{1/2}$ is the Frobenius norm. Indeed,

$$\left\| UU^\top - VV^\top \right\|_F^2 = 2r - 2\left\| U^\top V \right\|_F^2 = 2\sum_{i=1}^{r} \sin^2\theta_i. \tag{9}$$

It follows that $0 \le d_{\mathrm{chord}}(\mathcal{U}, \mathcal{V}) \le \sqrt{r}$, with distance zero if and only if the two subspaces coincide. Replacing the bases U and V by UO_1 and VO_2, respectively, where $O_1, O_2 \in \mathrm{O}(r)$, leaves the corresponding projection matrices and the distance unchanged. Thus, the chordal distance is independent of the orthonormal bases chosen to represent the two Grassmannian points [31]. For reference, Table 1 summarizes the main notation used throughout the remainder of the paper.

Table 1: Summary of main notation used throughout the paper.

Symbol	Description
S	A genomic sequence
$\mathcal{K} \subset \mathbb{N}_{>0}$	Finite, nonempty set of k-mer orders
$k \in \mathcal{K}$	A k-mer order
$m_{\mathcal{K}} = \sum_{k\in\mathcal{K}} 4^k$	Number of k-mer words across these orders
T	Number of filtration steps
$\mathcal{G}$	Finite, nonempty set of descriptor types
$g \in \mathcal{G}$	A descriptor type (Def. 2.1)
$G_{S,g}^{(k)} \in \mathbb{R}^{4^k \times T}$	k-mer topology feature block (Def. 2.1)
$s_{g,k}$	Dataset-level RMS normalization scale
$c_{g,k} = \sqrt{w_k}/\max(s_{g,k}, \varepsilon)$	Normalization weight for descriptor g and order k
$q = \lvert\mathcal{G}\rvert$	Number of descriptor types
$n = qm_{\mathcal{K}}$	Ambient feature dimension
$Z_S \in \mathbb{R}^{n\times T}$	Normalized, stacked feature matrix
r	Retained rank
$Z_S = U_S\Sigma_S V_S^\top$	Truncated singular value decomposition of Z_S
$\mathrm{Gr}(r, n)$	Grassmannian of r-dim. subspaces of $\mathbb{R}^n$ (Def. 2.2)
$\mathrm{span}(U_S) \in \mathrm{Gr}(r, n)$	GrassTop representation of S
$d_{\mathrm{chord}}(S, R)$	Grassmannian chordal distance (Eq. 8)
$\lVert Z_S - Z_R\rVert_F$	Frobenius distance between unprojected feature matrices

3 The GrassTop Framework

GrassTop is a framework for representing genomes as subspaces derived from multiscale topological and spectral descriptors of k-mer positional patterns. For each genome, the descriptor blocks are normalized and assembled before a retained singular subspace is extracted. This subspace defines a point on a Grassmannian, so two genomes can be compared through a distance between their corresponding Grassmannian points. Figure 1 presents the overall framework. Section 3.1 defines the construction, Section 3.2 establishes its main geometric properties, and Section 3.3 describes its computational cost.

3.1 GrassTop construction

Let $\mathcal{K} \subset \mathbb{N}_{>0}$ denote a finite, nonempty set of k-mer orders, and let $\mathcal{G}$ denote a finite, nonempty set of descriptor types as defined in Section 2.1. Starting from the k-mer topology descriptors of Section 2.1, GrassTop assembles the descriptor blocks, extracts a rank-r subspace, and compares the resulting genome representations with a distance d_{Gr} on the Grassmannian. The construction has four steps: feature extraction, normalization and stacking, Grassmannian embedding, and subspace comparison.

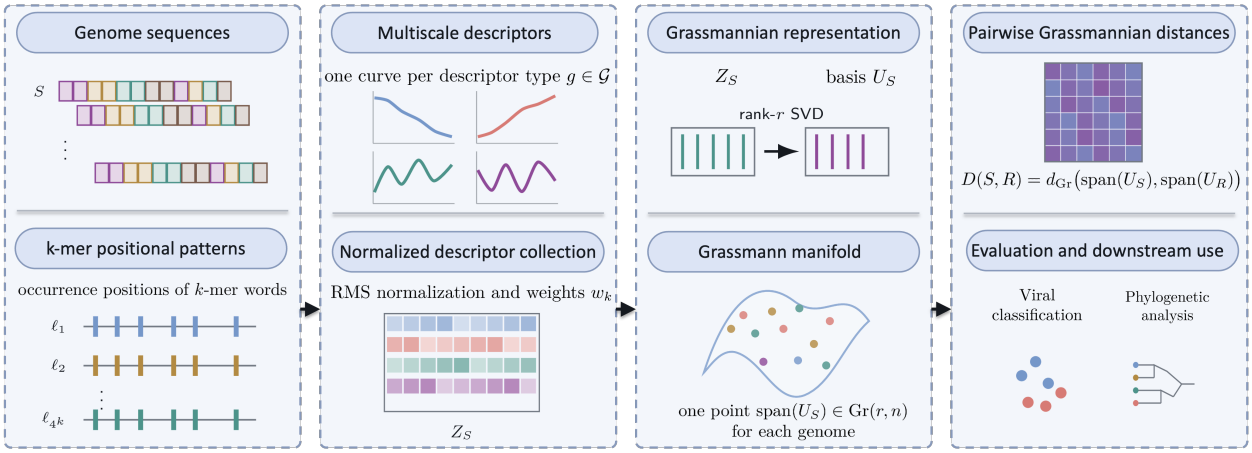

Figure 1: Overall GrassTop framework. For each genome, the occurrence positions of k-mer words are used to compute multiscale descriptors. The normalized descriptor collection is represented by a rank-r subspace on a Grassmann manifold. Pairwise Grassmannian distances between these subspaces provide the input for classification and phylogenetic analysis.

Step 1 (Feature extraction). For a sequence S, the k-mer topology feature blocks $G_{S,g}^{(k)}$ are computed for $k \in \mathcal{K}$ and $g \in \mathcal{G}$, as defined in Section 2.1. Each block records one descriptor type over the common filtration steps.

Step 2 (Normalization and stacking). Each block $G_{S,g}^{(k)}$ is normalized by an RMS scale $s_{g,k}$ and a k-dependent weight $c_{g,k} = \sqrt{w_k}/\max(s_{g,k}, \varepsilon)$, where $w_k > 0$ is the block weight for order k: it sets how much each k-mer order contributes to the assembled matrix Z_S relative to the other orders, independently of the RMS rescaling. The values of w_k used in the experiments are given in Section 4.1. The normalized blocks are then vertically stacked over (g, k) into one matrix

$$Z_S \in \mathbb{R}^{qm_{\mathcal{K}} \times T},$$

where $q = |\mathcal{G}|$ and $m_{\mathcal{K}} = \sum_{k \in \mathcal{K}} 4^k$. Let $n = qm_{\mathcal{K}}$ denote this ambient feature dimension. The scaling balances blocks from different descriptor types and k-mer orders before the subspace is extracted.

Step 3 (Rank-r Grassmannian embedding). For a retained rank $1 \le r \le \min(n, T)$, let $Z_S = U_S \Sigma_S V_S^\top$ denote a rank-r truncated singular value decomposition. GrassTop maps S to $\mathrm{span}(U_S) \in \mathrm{Gr}(r, n)$, the subspace spanned by the leading left singular vectors. The singular values Σ_S and right singular vectors V_S are not part of the Grassmannian representation.

Step 4 (Grassmannian distance). Let d_{Gr} be a distance on $\mathrm{Gr}(r, n)$. The distance between sequences S and R is defined as

$$D(S, R) = d_{\mathrm{Gr}}\big(\mathrm{span}(U_S), \mathrm{span}(U_R)\big).$$

For the chordal distance of Eq. (8), this becomes $D(S, R) = d_{\mathrm{chord}}(S, R)$. Other Grassmannian distances can be used without changing the representation.

Remark 3.1 (Framework specification)**.** *An instance of GrassTop is specified by its k-mer orders, descriptor types, filtration, block weights, retained rank, normalization scales, and Grassmannian distance. These*

quantities are fixed before genomes are represented or compared. Under a fixed specification, the mapping and pairwise comparison are deterministic and contain no learned weights. The specification used in the experiments is given in Section 4.1.

3.2 Geometric properties of the representation

The GrassTop representation is determined by the leading left singular subspace of Z rather than by a particular singular-vector basis. This construction yields the invariance and equivariance properties stated below. Define

$$\Phi_r(Z) = \mathrm{span}(U_r),$$

where U_r contains the r leading left singular vectors of Z.

Proposition 3.1 (Invariance and equivariance of the GrassTop embedding)**.** *Let $Z \in \mathbb{R}^{n\times T}$ and $1 \le r < \min(n, T)$ satisfy $\sigma_r(Z) > \sigma_{r+1}(Z)$, so that its leading r-dimensional left singular subspace is unique. For any nonzero scalar a, any $Q \in \mathrm{O}(T)$, and any $A \in \mathrm{O}(n)$,*

$$\Phi_r(aZQ) = \Phi_r(Z), \tag{10}$$

$$\Phi_r(AZ) = A\Phi_r(Z). \tag{11}$$

Consequently, independent nonzero rescaling and right-orthogonal transformation of two descriptor matrices do not change their GrassTop chordal distance. A common left-orthogonal transformation also leaves that distance unchanged.

Proof. The left singular subspace of Z is the eigenspace of $ZZ^\top$ associated with its r largest eigenvalues. Since

$$(aZQ)(aZQ)^\top = a^2 ZZ^\top,$$

the leading eigenspace is unchanged, which proves Eq. (10). Also, $(AZ)(AZ)^\top = A(ZZ^\top)A^\top$, so its leading eigenspace is the image under A of the leading eigenspace of $ZZ^\top$, proving Eq. (11). The distance statements follow from Eq. (8) and the invariance of the Frobenius norm under orthogonal transformations. □

The proposition also clarifies the role of normalization. GrassTop is invariant to overall scaling of a descriptor matrix, but not to arbitrary rescaling of individual rows or descriptor blocks; such transformations can change $ZZ^\top$ and hence the represented subspace. Block normalization and the retained rank are therefore structural parts of the representation rather than properties removed by the Grassmannian embedding.

3.3 Computational cost

GrassTop uses the persistent-homology and persistent-Laplacian calculations of [8] to obtain the k-mer topology descriptors. Their cost depends on the k-mer orders, word occurrences and positions, filtration resolution, and the topological or spectral quantities being computed. The analysis below focuses on the normalization, assembly, subspace computation, and distance evaluation applied after descriptor construction.

Let $n = qm_{\mathcal{K}}$ be the number of rows in the assembled descriptor array and let T be the number of filtration values. For each genome, normalization and assembly require $O(nT)$ operations. The implementation used in this study forms the $T \times T$ Gram matrix $Z_S^\top Z_S$, computes its eigendecomposition, and recovers the r leading left singular vectors. These operations require, respectively, $O(nT^2)$, $O(T^3)$, and $O(nTr)$ time. The working memory for the assembled array, Gram matrix, and retained basis is $O(nT + T^2 + nr)$. In the rank-deficient case, the implementation instead uses a dense SVD, whose time complexity is $O(nT \min(n, T))$.

Once the subspace representations have been constructed, computing the chordal distance between two genomes requires $O(nr^2)$ operations. For a collection of N genomes, all pairwise distances therefore require $O(N^2nr^2)$ operations and $O(N^2)$ storage if the complete distance matrix is retained. Estimating shared

normalization factors requires a single pass over the relevant descriptor arrays. After these factors have been fixed, feature construction and subspace computation can be performed independently for each genome.

4 Experiments

We evaluated GrassTop through viral-family classification, phylogenetic clustering, and sequence perturbation. For classification, pairwise chordal distances were used for 5-nearest-neighbor prediction of viral-family labels. For phylogenetic analysis, the same distances were used to construct UPGMA trees, which were evaluated against known taxonomic or lineage groups. The perturbation experiment changed bases at specified rates and compared how well GrassTop and the underlying descriptors preserved source identity and group labels. The classification and clustering results were compared with published alignment-free methods.

4.1 Datasets and evaluation

All experiments use the same k-mer orders, filtration resolution, block weights, retained rank, and Grassmannian distance. Specifically, $\mathcal{K} = \{1, \ldots, 5\}$, $T = 50$ filtration steps, $w_k = 2^{-(5-k)}$ [8], rank $r = 10$, and the chordal distance. For this configuration, $m_{\mathcal{K}} = \sum_{k=1}^{5} 4^k = 1364$. Classification uses the four descriptor types B, E, MEANP, and STDP; phylogenetic clustering uses B alone; and the perturbation experiment uses B, MEANP, and STDP. For each task, the RMS scales $s_{g,k}$ are estimated once from the complete dataset without class labels and are then held fixed throughout the analysis, including all cross-validation folds in the classification task.

4.1.1 Classification datasets and evaluation

Four NCBI viral-genome datasets were used: NCBI 2020, NCBI 2022, NCBI 2024, and NCBI 2024 (All) [8]. Families containing fewer than 15 sequences were removed before the data were split. Table 2 gives the numbers of sequences and families remaining in each dataset.

Table 2: Dataset sizes after removing families with fewer than 15 sequences.

Dataset	Sequences	Families
NCBI 2020	6,810	57
NCBI 2022	11,066	78
NCBI 2024	11,635	109
NCBI 2024 (All)	13,160	120

Each filtered dataset was evaluated by stratified 5-fold cross-validation with 30 random seeds. For each test sequence, the five training sequences with the smallest GrassTop distances were identified, and their majority family was assigned to the test sequence. Accuracy (ACC), balanced accuracy (BA), F1, one-vs-rest AUC-ROC, recall, and precision were calculated for each fold. Results were averaged over the 150 cross-validation folds. The reference methods were the natural vector method (NVM) [25], feature-frequency profiles compared by Jensen–Shannon divergence (FFP-JS) [10, 23], feature-frequency profiles compared by Kullback–Leibler divergence (FFP-KL) [27], the Markov k-string method [20], and the Fourier power spectrum method (FPS) [7]. Their values in Section 4.2.1 were taken from [8], which used the same evaluation procedure.

4.1.2 Phylogenetic datasets and tree evaluation

Four datasets were used for phylogenetic clustering: human rhinovirus (HRV, n=116, four labels), mammalian mitochondrial genomes (n=41, eight labels), Ebolavirus (n=59, five labels), and SARS-CoV-2 (n=44,

eight lineage groups) [26]. The HRV, mitochondrial, and Ebolavirus datasets contain every accession in the published lists. The 44 SARS-CoV-2 sequences and their lineage labels were retrieved from GISAID using the published EPI_ISL accessions.

For each dataset, GrassTop distances were used to construct a UPGMA tree. Labels were not used to calculate distances or construct the tree. Tree purity was calculated from Eqs. 22–24 of Ref. [26]. Let $\mathcal{L}$ be the set of labels, let S_ℓ be the set of leaves with label ℓ, and let $n_\ell = |S_\ell|$. The maximal pure subtrees for label ℓ partition S_ℓ into $S_{\ell,1}, \ldots, S_{\ell,m_\ell}$. The tree-level purity reported in Table 7 is

$$\mathrm{Purity}(T) = \frac{1}{|\mathcal{L}|} \sum_{\ell \in \mathcal{L}} \sum_{j=1}^{m_\ell} \left(\frac{|S_{\ell,j}|}{n_\ell} \right)^2 . \tag{12}$$

A label has purity 1 when all of its leaves belong to one pure subtree; fragmentation across several pure subtrees gives a smaller value.

The five Ebolavirus reference entries marked † in Table 7 use the clade-consistency precision reported by [8], rather than Eq. (12). For a label ℓ, let C_ℓ be the leaf set of the smallest clade containing all leaves in S_ℓ. Its precision is

$$\mathrm{Prec}(\ell) = \frac{|S_\ell|}{|C_\ell|}. \tag{13}$$

Thus, the score is 1 for a label exactly when its smallest containing clade has no leaves from other labels. The cited study reports a value of 1.00 for each of the five reference methods on Ebolavirus. These values are retained as published but are not directly comparable with the GrassTop purity because the scoring definitions differ.

4.1.3 Sequence perturbation experiment

The same four phylogenetic datasets were used in the sequence perturbation experiment. At each perturbation rate p, every A, C, G, or T position was independently changed with probability p. The original base at each selected position was replaced with one of the other three bases, chosen uniformly at random. The rates were

$$p \in \{0.0001, 0.0005, 0.001, 0.005, 0.01, 0.02, 0.05, 0.1, 0.15, 0.25, 0.4\}.$$

For example, at $p = 0.001$, a sequence of length 10,000 has 10 changed positions on average. If position 237 is selected and contains A, it may be changed to G, while every position not selected remains unchanged.

One original sequence was sampled from each label. At each rate, the procedure above was repeated independently five times for every sampled sequence. The selected positions and replacement bases could therefore differ among the five perturbed sequences. No bases were inserted or deleted, so all sequences retained their original length. For each dataset and rate, this gave 20 perturbed sequences for HRV, 25 for Ebolavirus, and 40 each for the mitochondrial and SARS-CoV-2 datasets. GrassTop and the descriptors before subspace projection were computed from the same perturbed sequences using B, MEANP, and STDP. For both GrassTop and these descriptors, the five nearest neighbors of each perturbed sequence were selected from all original sequences.

Label-preservation. A perturbed sequence is counted as label-preserved when the majority label among its five nearest neighbors equals the label of its original sequence. The reported score is the fraction of perturbed sequences satisfying this condition at a given perturbation rate.

Self-preservation. A perturbed sequence is counted as self-preserved when its original sequence occurs among its five nearest neighbors. The reported score is the fraction of perturbed sequences satisfying this condition at a given perturbation rate.

We also measured the distance from each perturbed sequence to its original sequence. We used the chordal distance for GrassTop (Eq. (8)) and the Frobenius distance for the descriptors before projection. Each distance was divided by the mean pairwise distance among the original sequences, calculated separately for GrassTop and the descriptors. A normalized value of 1 therefore equals the mean distance between original sequences for the corresponding method. The same original and perturbed sequences were used for all three measurements.

4.2 Results

The following subsections present the experimental results for viral-family classification, phylogenetic clustering, and sequence perturbation.

4.2.1 Classification benchmark

GrassTop has the largest displayed value for each of the six classification metrics in all four datasets (Tables 3–6). The reference values for NVM [25], FFP-JS [10, 23], FFP-KL [27], Markov k-string [20], and FPS [7] were taken from Table 1 of [8].

Table 3: 5-NN classification results (macro-averaged over 5-fold $\times$ 30-seed CV), NCBI 2020. The first five rows are reported in Table 1 of [8]. Bold indicates the largest displayed value in each column.

Method	ACC	BA	F1	AUC-ROC	Recall	Precision
NVM	0.847	0.807	0.809	0.960	0.807	0.840
FFP-JS	0.821	0.790	0.781	0.954	0.790	0.814
FFP-KL	0.819	0.789	0.780	0.954	0.789	0.814
Markov	0.713	0.644	0.622	0.905	0.644	0.668
FPS	0.714	0.637	0.633	0.917	0.637	0.665
GrassTop	**0.9131**	**0.8909**	**0.8925**	**0.9798**	**0.8909**	**0.9046**

Table 4: 5-NN classification results, NCBI 2022. The first five rows are reported in Table 1 of [8]. Bold indicates the largest displayed value in each column.

Method	ACC	BA	F1	AUC-ROC	Recall	Precision
NVM	0.852	0.747	0.750	0.935	0.747	0.791
FFP-JS	0.830	0.740	0.733	0.937	0.740	0.769
FFP-KL	0.832	0.743	0.735	0.934	0.743	0.771
Markov	0.724	0.593	0.577	0.876	0.593	0.617
FPS	0.723	0.588	0.580	0.890	0.588	0.603
GrassTop	**0.9040**	**0.8229**	**0.8288**	**0.9593**	**0.8229**	**0.8656**

Table 5: 5-NN classification results, NCBI 2024. The first five rows are reported in Table 1 of [8]. Bold indicates the largest displayed value in each column.

Method	ACC	BA	F1	AUC-ROC	Recall	Precision
NVM	0.814	0.729	0.738	0.933	0.729	0.789
FFP-JS	0.796	0.724	0.712	0.936	0.724	0.744
FFP-KL	0.796	0.727	0.714	0.932	0.727	0.747
Markov	0.633	0.589	0.554	0.876	0.589	0.573
FPS	0.660	0.561	0.560	0.882	0.561	0.593
GrassTop	**0.8805**	**0.8135**	**0.8228**	**0.9590**	**0.8135**	**0.8645**

Table 6: 5-NN classification results, NCBI 2024 (All). The first five rows are reported in Table 1 of [8]. Bold indicates the largest displayed value in each column.

Method	ACC	BA	F1	AUC-ROC	Recall	Precision
NVM	0.809	0.729	0.738	0.931	0.729	0.788
FFP-JS	0.799	0.721	0.711	0.935	0.721	0.745
FFP-KL	0.799	0.724	0.712	0.931	0.724	0.745
Markov	0.638	0.589	0.555	0.876	0.589	0.575
FPS	0.651	0.561	0.559	0.879	0.561	0.591
GrassTop	**0.8788**	**0.8165**	**0.8232**	**0.9588**	**0.8165**	**0.8629**

Within each dataset, NVM is the strongest of the five reference methods on five or six of the six metrics; the exception is AUC-ROC on NCBI 2022, 2024, and 2024 (All), where FFP-JS is marginally higher than NVM. Measured against the strongest reference value in each column, GrassTop's margin depends more on the metric than on the dataset. The margin is smallest and most stable for AUC-ROC, ranging from 0.0198 (NCBI 2020) to 0.0238 (NCBI 2024 All), because all five reference methods already score above 0.87 on this metric. The margin is largest for balanced accuracy, F1, and recall, ranging from about 0.076 to 0.088 across the four datasets; balanced accuracy and recall take identical values in every row because macro-averaged recall coincides with balanced accuracy under this evaluation protocol. The margin for accuracy and precision falls between the other two groups, at roughly 0.052–0.070 for accuracy and 0.065–0.076 for precision.

These comparisons concern the complete GrassTop representation, including the selected descriptors, normalization, retained rank, and chordal distance. Because the published methods use different feature constructions, the results do not isolate the effect of the subspace representation alone.

4.2.2 Phylogenetic clustering purity

Each of the four GrassTop trees has an average purity of 1.0 under the stated purity measure. Table 7 places these results alongside published alignment-free reference values. For SARS-CoV-2, mammalian mitochondrial genomes, and HRV, the reference values were read from the bars in Fig. 2d–f of [26]. The Ebolavirus values are from Table 2 of [8] and use a different clade-consistency measure; they are included for context but not as a direct numerical comparison.

GrassTop is above the five displayed reference values for SARS-CoV-2 and mammalian mitochondrial genomes and equals the FPS value of 1.0 for HRV. For Ebolavirus, GrassTop reaches 1.0 under the purity

measure used here, while each reference method reaches 1.0 under the related measure reported in [8]. The equality of these Ebolavirus values does not establish equivalent performance because the measures differ.

Table 7: UPGMA clustering scores. Unmarked values use the tree purity in Eq. (12); baseline values for the first three datasets are read from Fig. 2d–f of [26]. Values marked † are the clade-consistency precision scores reported in Table 2 of [8] and follow Eq. (13). GrassTop uses the Betti-0 descriptor type and rank $r = 10$. Bold identifies the GrassTop value; daggered and unmarked values should not be compared as if they used the same score.

Dataset	Method	Reported score
SARS-CoV-2	NVM	0.372
	FFP-JS	0.835
	FFP-KL	0.795
	FPS	0.267
	Markov (MKS)	0.828
	GrassTop	**1.0000**
Mammalian mitochondrial	NVM	0.906
	FFP-JS	0.876
	FFP-KL	0.876
	FPS	0.953
	Markov (MKS)	0.732
	GrassTop	**1.0000**
Human rhinovirus (HRV)	NVM	0.878
	FFP-JS	0.745
	FFP-KL	0.795
	FPS	1.000
	Markov (MKS)	0.337
	GrassTop	**1.0000**
Ebolavirus	NVM†	1.00
	FFP-JS†	1.00
	FFP-KL†	1.00
	FPS†	1.00
	Markov†	1.00
	GrassTop	**1.0000**

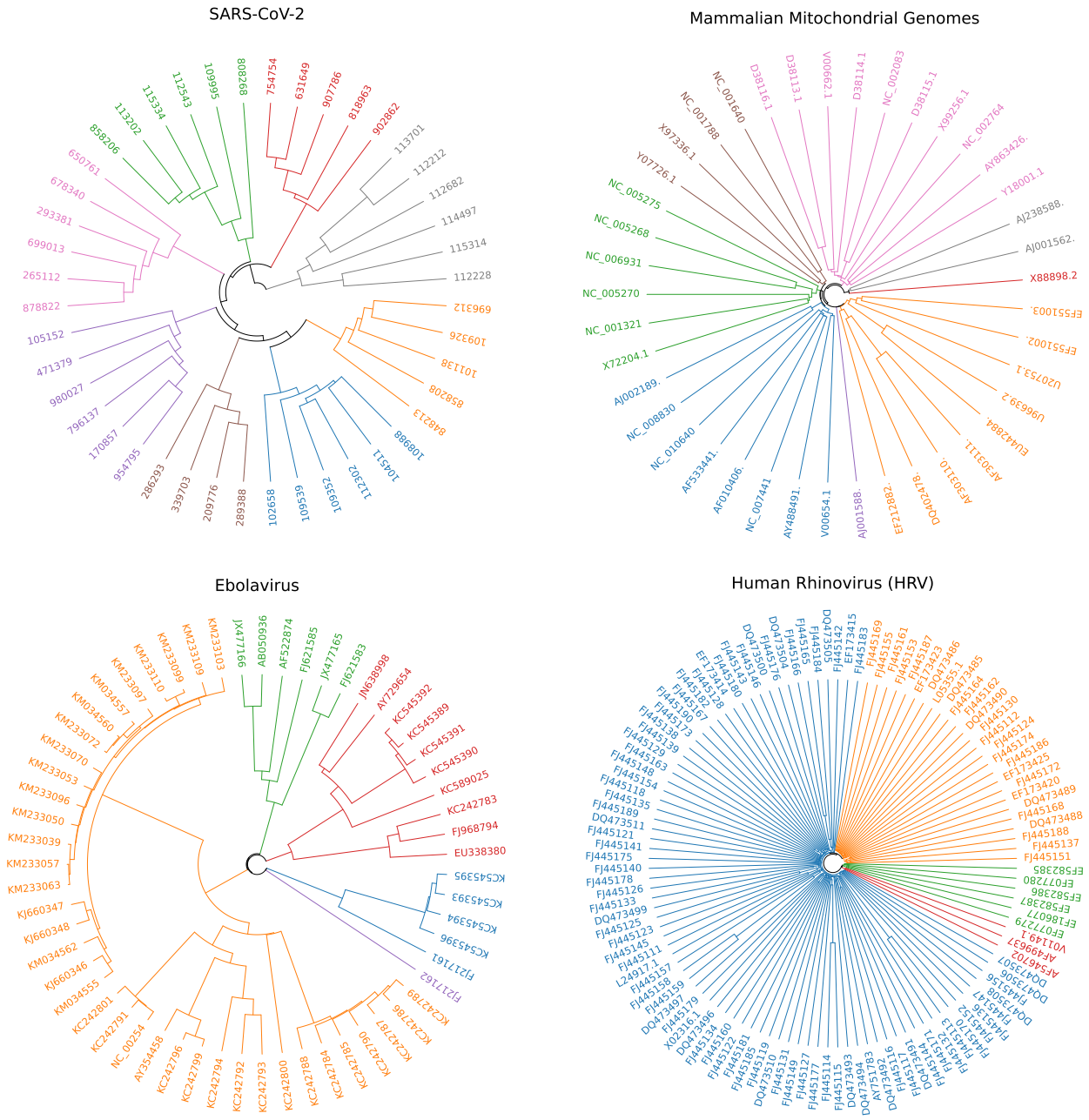

Figure 2: Circular UPGMA trees constructed from GrassTop distances. Branches are colored by the ground-truth label of the largest pure subtree to which they belong and are black when a merge joins different labels. Top-left: SARS-CoV-2 (n=44, lineage). Top-right: mammalian mitochondrial genomes (n=41, order). Bottom-left: Ebolavirus (n=59, species: BDBV/EBOV/RESTV/SUDV/TAFV). Bottom-right: human rhinovirus (n=116, HRV-A/HRV-B/HRV-C and the HEV outgroup).

4.2.3 Stability under sequence perturbation

Across the four selected perturbation rates in Appendix Tables A1 and A2 (32 dataset-rate-measure combinations in total: 4 datasets × 4 rates × 2 measures), GrassTop matches or exceeds comparison based on the Frobenius distance between the unprojected feature matrices in 29 of 32 combinations, with a strict advantage in 19 and a tie in 10. The three exceptions are small in absolute size and occur either at the highest tested perturbation rate, where both representations are already heavily degraded (SARS-CoV-2 label-preservation at rate 0.40, a 0.02 gap, and self-preservation at rate 0.40, a 0.09 gap), or in the 20-sequence HRV sample (label-preservation at rate 0.25). Figure 3 shows label- and self-preservation across the full 11 perturbation rates.

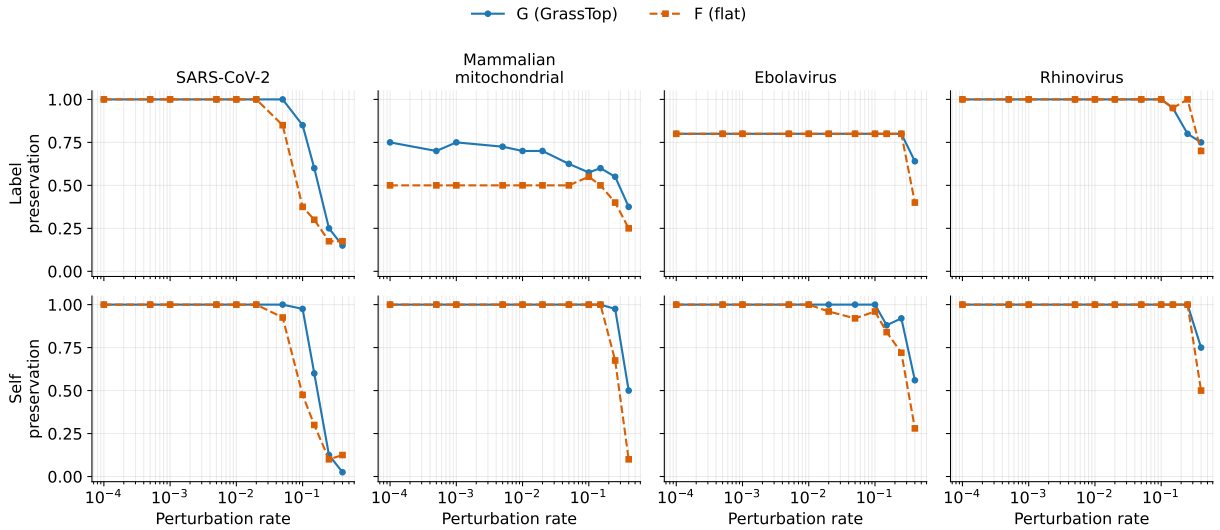

Figure 3: Label- and self-preservation over the 11 perturbation rates. Label-preservation (top) is the fraction of perturbed sequences whose 5-NN majority vote recovers the original label; self-preservation (bottom) is the fraction for which the original sequence remains among the five nearest neighbors. The perturbation-rate axis is logarithmic. Solid curves denote GrassTop and dashed curves denote comparison based on the Frobenius distance between the unprojected feature matrices.

For SARS-CoV-2, GrassTop has higher preservation over most of the perturbation-rate grid. At rate 0.10, label-preservation is 0.85 for GrassTop and 0.375 for comparison based on the unprojected feature matrices, while self-preservation is 0.975 and 0.475, respectively. At rate 0.40, label-preservation is low for both comparisons and is slightly higher when the unprojected feature matrices are compared by Frobenius distance (0.17 versus 0.15). For mammalian mitochondrial genomes, GrassTop has higher label-preservation at every sampled rate; the values at rate 0.25 are 0.55 and 0.40. Values below 1 at the lowest perturbation rates can occur because preservation is evaluated by 5-NN within a pool of 41 sequences assigned to eight labels; they do not necessarily result from the perturbation.

For Ebolavirus, both representations have label-preservation of 0.80 from rate 0.0001 through 0.25. GrassTop has higher self-preservation from rate 0.02 onward and is higher on both measures at rate 0.40. For HRV, the preservation values are equal through rate 0.15. At rate 0.25, label-preservation is 1.00 for comparison based on the Frobenius distance between the unprojected feature matrices and 0.80 for GrassTop; at rate 0.40, GrassTop is higher on both measures. Each HRV value is based on 20 perturbed sequences, so these differences do not locate a precise crossover rate.

The normalized distances to the original sequences provide a complementary comparison (Figure 4; Appendix Table A3). In all four datasets, the normalized chordal distance (GrassTop) falls below the normalized Frobenius distance between the unprojected feature matrices once the perturbation rate is high enough, consistent with the upper bound $\sqrt{r}$ for the chordal distance and the absence of a corresponding upper bound for the Frobenius distance. The rate at which this crossover occurs, and the size of the gap it

opens by rate 0.40, both depend on the dataset. For SARS-CoV-2 the crossover is earliest, at rate 0.0050, and the gap is largest by rate 0.40: a ratio of about 3.1 (13.315 versus 4.262). For Ebolavirus the crossover occurs at rate 0.15, and for mammalian mitochondrial genomes and HRV it occurs later, at rate 0.25; the ratio at rate 0.40 is correspondingly smaller: about 1.5 for Ebolavirus (1.973 versus 1.341), 1.3 for mammalian mitochondrial genomes (1.325 versus 1.057), and 1.2 for HRV (1.261 versus 1.051). Because the datasets differ in sequence length, label structure, and within-group diversity, this experiment does not determine why the crossover rate and the resulting gap size differ across datasets.

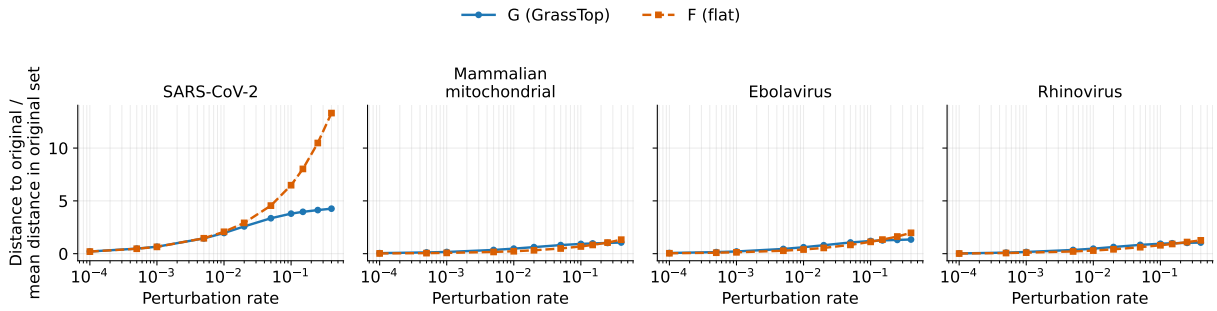

Figure 4: Mean distance from each perturbed sequence to its original sequence, normalized by the mean pairwise distance among the original sequences. The perturbation-rate axis is logarithmic. Solid curves denote GrassTop and dashed curves denote comparison based on the Frobenius distance between the unprojected feature matrices; shaded regions show the interquartile range at each rate.

5 Discussion

Across the three empirical evaluations in Section 4, GrassTop matches or exceeds the compared alignment-free methods on nearly every reported measure: it is above all five reference methods on each of the six classification metrics on all four NCBI corpora (Section 4.2.1); it attains average label purity 1.0 on all four phylogenetic datasets (Section 4.2.2); and under sequence perturbation, it matches or exceeds comparison based on the Frobenius distance between the unprojected feature matrices in 29 of the 32 selected dataset-rate-measure combinations reported in Section 4.2.3. These results evaluate the complete GrassTop representation as a unit, with the classification and phylogenetic baselines coming from separately published implementations rather than a shared codebase. A natural next step is an ablation that holds the descriptors, normalization, and rank fixed while varying only the subspace/distance step, which would isolate how much of the observed advantage is attributable to the Grassmannian embedding itself.

Two directions can further strengthen this evidence. First, the tree purity of Eq. (12) is a targeted measure of label recovery; extending the evaluation with branch-length- or divergence-time-aware criteria against established evolutionary models is a natural next step, complementing the label-recovery evidence reported here. Second, the distance behavior in the perturbation experiment is consistent with the different bounds of the two distance functions. The chordal distance is bounded above by $\sqrt{r}$ (Section 2.2), whereas the Frobenius distance between the unprojected feature matrices has no corresponding upper bound. In all four datasets, GrassTop's normalized distance to the original sequence eventually grows more slowly than that obtained by direct comparison of the unprojected feature matrices. The perturbation rate at which this crossover occurs and the size of the resulting gap differ sharply by dataset; identifying what drives this dataset dependence is a further direction worth pursuing.

The scope of the evidence is defined by the reported configuration and protocols. The experiments use $r = 10$ and task-specific descriptor-type sets; other choices are allowed by the framework but are not evaluated here. The classification baselines are published values rather than results from a shared implementation, and several phylogenetic values were estimated from a published figure. The normalization scales are computed from each full classification corpus without using labels, so held-out observations contribute to this

preprocessing step. Finally, preservation proportions are based on 20–40 perturbed records per rate and dataset. These conditions limit the comparison to the datasets and settings reported in this study.

6 Conclusion

We presented GrassTop as a multiscale topological and spectral method for viral classification and phylogenetic analysis. GrassTop captures k-mer positional patterns of a sequence by a subspace on a Grassmannian. This formulation permits genome comparison with distances on the Grassmannian and is not restricted to the descriptor types, k-mer orders, rank, or distance used in the reported experiments. In these experiments, GrassTop exceeds five published reference methods to cross the viral-family classification results displayed and recovers the groups supplied with average purity 1.0 in four UPGMA datasets. Under sequence perturbation, it matches or exceeds comparison based on the Frobenius distance between the unprojected feature matrices in the large majority of the tested dataset-rate-measure combinations (29 of 32), with the size of the advantage varying by dataset. Taken together, the results support GrassTop for viral classification and phylogenetic analysis tasks examined here while keeping its conclusions within the tested configurations and datasets. GrassTop can be applied to a variety of tasks involving genome representation and analysis, including antigenic analysis of seasonal virus vaccines and protein-nucleic acid binding prediction.

Data and Code Availability

The code used in this study is available at https://github.com/XiangXiangJY/GrassTop. The public benchmark datasets can be obtained from the CAKL repository at https://github.com/FaisalSuwayyid/CAKL. SARS-CoV-2 sequences are subject to the GISAID Terms of Use and are not redistributed.

Acknowledgments

This work was supported in part by NIH grant R01AI164266, The University of Georgia (UGA), and Georgia Research Alliance.

A Numerical results for the sequence perturbation experiment

This appendix gives numerical values that complement the perturbation curves in the main text. Tables A1 and A2 contain label- and self-preservation at four selected perturbation rates from Figure 3. Table A3 contains the normalized mean distances plotted in Figure 4 for all 11 rates. The evaluation definitions and sampling design are given in Section 4.1.3.

Table A1: Label-preservation at four selected perturbation rates. Values are the fractions of perturbed sequences for which the 5-NN majority vote recovers the original label. G denotes GrassTop, and F denotes comparison based on the Frobenius distance between the unprojected feature matrices.

	rate= 0.05		rate= 0.15		rate= 0.25		rate= 0.4	
Dataset	G	F	G	F	G	F	G	F
SARS-CoV-2	1.00	0.85	0.60	0.30	0.25	0.17	0.15	0.17
Mito. (mammal.)	0.62	0.50	0.60	0.50	0.55	0.40	0.38	0.25
Ebolavirus	0.80	0.80	0.80	0.80	0.80	0.80	0.64	0.40
Rhinovirus	1.00	1.00	0.95	0.95	0.80	1.00	0.75	0.70

Table A2: Self-preservation at four selected perturbation rates. Values are the fractions of perturbed sequences whose original sequence remains among their five nearest neighbors. G denotes GrassTop, and F denotes comparison based on the Frobenius distance between the unprojected feature matrices.

	rate= 0.05		rate= 0.15		rate= 0.25		rate= 0.4	
Dataset	G	F	G	F	G	F	G	F
SARS-CoV-2	1.00	0.93	0.60	0.30	0.12	0.10	0.03	0.12
Mito. (mammal.)	1.00	1.00	1.00	1.00	0.97	0.68	0.50	0.10
Ebolavirus	1.00	0.92	0.88	0.84	0.92	0.72	0.56	0.28
Rhinovirus	1.00	1.00	1.00	1.00	1.00	1.00	0.75	0.50

Table A3: Normalized mean distance from each perturbed sequence to its original sequence over all 11 perturbation rates in Figure 4. Each value is divided by the mean pairwise distance among the original sequences and rounded to three decimal places. G denotes GrassTop, and F denotes comparison based on the Frobenius distance between the unprojected feature matrices. The numbers of perturbed sequences per rate are 40, 40, 25, and 20 for SARS-CoV-2, mammalian mitochondrial genomes, Ebolavirus, and HRV, respectively.

	SARS-CoV-2		Mito.		Ebolavirus		Rhinovirus	
Rate	G	F	G	F	G	F	G	F
0.0001	0.206	0.198	0.052	0.023	0.065	0.040	0.023	0.014
0.0005	0.477	0.466	0.119	0.053	0.149	0.091	0.100	0.061
0.0010	0.658	0.645	0.161	0.074	0.208	0.129	0.163	0.096
0.0050	1.445	1.458	0.353	0.163	0.448	0.280	0.352	0.211
0.0100	1.958	2.071	0.477	0.230	0.610	0.393	0.474	0.294
0.0200	2.580	2.915	0.621	0.321	0.801	0.545	0.632	0.412
0.0500	3.356	4.552	0.814	0.492	1.061	0.832	0.832	0.612
0.1000	3.791	6.485	0.925	0.683	1.203	1.119	0.940	0.795
0.1500	3.963	8.026	0.970	0.827	1.257	1.332	0.985	0.918
0.2500	4.127	10.479	1.015	1.051	1.302	1.623	1.026	1.102
0.4000	4.262	13.315	1.057	1.325	1.341	1.973	1.051	1.261

References

[1] Fan R. K. Chung. *Spectral Graph Theory*, volume 92 of *CBMS Regional Conference Series in Mathematics*. American Mathematical Society, Providence, RI, 1997.

[2] Alan Edelman, Tomás A. Arias, and Steven T. Smith. The geometry of algorithms with orthogonality constraints. *SIAM Journal on Matrix Analysis and Applications*, 20(2):303–353, 1998.

[3] Herbert Edelsbrunner, David Letscher, and Afra Zomorodian. Topological persistence and simplification. *Discrete & Computational Geometry*, 28:511–533, 2002.

[4] Hongsong Feng, Sean Cottrell, Yuta Hozumi, and Guo-Wei Wei. Multiscale differential geometry learning of networks with applications to single-cell RNA sequencing data. *Computers in Biology and Medicine*, 171:108211, 2024.

[5] Skylar A Gay, Gregory Ellison, Jianing Xu, Jialin Yang, Yiliang Wei, Shaoyuan Wu, Lili Yu, Christopher C Whalen, Jonathan Arnold, and Liang Liu. Phylogenetic inference of inter-population transmission rates for infectious diseases. *Briefings in Bioinformatics*, 25(4):bbae312, 2024.

[6] Gene H. Golub and Charles F. Van Loan. *Matrix Computations*. Johns Hopkins University Press, Baltimore, MD, 4 edition, 2013.

[7] Tung Hoang, Changchuan Yin, Hui Zheng, Chenglong Yu, Rong Lucy He, and Stephen S.-T. Yau. A new method to cluster DNA sequences using fourier power spectrum. *Journal of Theoretical Biology*, 372:135–145, 2015.

[8] Yuta Hozumi and Guo-Wei Wei. Revealing the shape of genome space via k-mer topology. *SIAM Journal on Life Sciences*, 1(2):310–332, 2026. arXiv:2412.20202.

[9] Jürgen Jost, Yuanlong L Xin, and Ling Yang. The geometry of grassmannian manifolds and bernstein type theorems for higher codimension. *ANNALI SCUOLA NORMALE SUPERIORE-CLASSE DI SCIENZE*, pages 1–39, 2016.

[10] Se-Ran Jun, Gregory E. Sims, Guohong A. Wu, and Sung-Hou Kim. Whole-proteome phylogeny of prokaryotes by feature frequency profiles: An alignment-free method with optimal feature resolution. *Proceedings of the National Academy of Sciences*, 107(1):133–138, 2010.

[11] Xiaoguang Li, Tao Zhou, Xingdong Feng, Shing-Tung Yau, and Stephen S.-T. Yau. Exploring geometry of genome space via grassmann manifolds. *The Innovation*, 5(5):100677, 2024.

[12] Jian Liu, Li Shen, Dong Chen, and Guo-Wei Wei. Topological sequence analysis of genomes: Delta complex approaches. *Foundations of Data Science*, 11:29–49, 2026.

[13] Xiang Liu, Huitao Feng, Jie Wu, and Kelin Xia. Persistent spectral hypergraph based machine learning (psh-ml) for protein-ligand binding affinity prediction. *Briefings in bioinformatics*, 22(5):bbab127, 2021.

[14] Yang Young Lu, Kujin Tang, Jie Ren, Jed A Fuhrman, Michael S Waterman, and Fengzhu Sun. Cafe: a c celerated a lignment-f r e e sequence analysis. *Nucleic acids research*, 45(W1):W554–W559, 2017.

[15] Zhenyu Meng and Kelin Xia. Persistent spectral-based machine learning (PerSpect ML) for protein–ligand binding affinity prediction. *Science Advances*, 7(19):eabc5329, 2021.

[16] Lin Mu, Kelin Xia, and Guo-Wei Wei. Geometric and electrostatic modeling using molecular rigidity functions. *Journal of Computational and Applied Mathematics*, 313:18–37, 2017.

[17] Frederik A Murphy, Claude M Fauquet, David HL Bishop, Said A Ghabrial, Audrey W Jarvis, Giovanni P Martelli, Mike A Mayo, and Max D Summers. *Virus taxonomy: classification and nomenclature of viruses*, volume 10. Springer Science & Business Media, 2012.

[18] Duc Duy Nguyen, Zixuan Cang, and Guo-Wei Wei. A review of mathematical representations of biomolecular data. *Physical Chemistry Chemical Physics*, 22(8):4343–4367, 2020.

[19] Theodore Papamarkou, Tolga Birdal, Michael Bronstein, Gunnar Carlsson, Justin Curry, Yue Gao, Mustafa Hajij, Roland Kwitt, Pietro Lio, Paolo Di Lorenzo, et al. Position: Topological deep learning is the new frontier for relational learning. *Proceedings of machine learning research*, 235:39529, 2024.

[20] Ji Qi, Bin Wang, and Bai-Lin Hao. Whole proteome prokaryote phylogeny without sequence alignment: A k-string composition approach. *Journal of Molecular Evolution*, 58(1):1–11, 2004.

[21] Yiming Ren and Guo-Wei Wei. Interpretability and representability of commutative algebra, algebraic topology, and topological spectral theory for real-world data. *Advanced Intelligent Discovery*, page e202500207, 2025.

[22] Cong Shen, Jiawei Luo, and Kelin Xia. Molecular geometric deep learning. *Cell Reports Methods*, 3(2):100621, 2023.

[23] Gregory E. Sims, Se-Ran Jun, Guohong A. Wu, and Sung-Hou Kim. Alignment-free genome comparison with feature frequency profiles (FFP) and optimal resolutions. *Proceedings of the National Academy of Sciences*, 106(8):2677–2682, 2009.

[24] Zhe Su, Xiang Liu, Layal Bou Hamdan, Vasileios Maroulas, Jie Wu, Gunnar Carlsson, and Guo-Wei Wei. Topological data analysis and topological deep learning beyond persistent homology: a review. *Artificial intelligence review*, 59(2):58, 2025.

[25] Nan Sun, Shaojun Pei, Lily He, Changchuan Yin, Rong Lucy He, and Stephen S.-T. Yau. Geometric construction of viral genome space and its applications. *Computational and Structural Biotechnology Journal*, 19:4226–4234, 2021.

[26] Faisal Suwayyid, Yuta Hozumi, Hongsong Feng, Mushal Zia, JunJie Wee, and Guo-Wei Wei. CAKR: Commutative algebra k-mer representation of genomics. *Nature Communications*, pages https://doi.org/10.1038/s41467–026–76429–z, 2026. arXiv:2508.09406, August 14, 2025.

[27] Susana Vinga and Jonas Almeida. Alignment-free sequence comparison: A review. *Bioinformatics*, 19(4):513–523, 2003.

[28] Rui Wang, Duc Duy Nguyen, and Guo-Wei Wei. Persistent spectral graph. *International Journal for Numerical Methods in Biomedical Engineering*, 36(9):e3376, 2020.

[29] JunJie Wee and Jian Jiang. A review of topological data analysis and topological deep learning in molecular sciences. *Journal of Chemical Information and Modeling*, 65(23):12691, 2025.

[30] Kelin Xia and Guo-Wei Wei. Persistent homology analysis of protein structure, flexibility, and folding. *International Journal for Numerical Methods in Biomedical Engineering*, 30(8):814–844, 2014.

[31] Ke Ye and Lek-Heng Lim. Schubert varieties and distances between subspaces of different dimensions. *SIAM Journal on Matrix Analysis and Applications*, 37(3):1176–1197, 2016.

[32] Andrzej Zielezinski, Susana Vinga, Jonas Almeida, and Wojciech M Karlowski. Alignment-free sequence comparison: benefits, applications, and tools. *Genome biology*, 18(1):186, 2017.

[33] Afra Zomorodian and Gunnar Carlsson. Computing persistent homology. *Discrete & Computational Geometry*, 33:249–274, 2005.